Communications on Applied Nonlinear Analysis
ISSN: 1074-133X
Vol 32 No. 10s (2025)

Probing Nonlinear Optical Phenomena in Metal-Organic Frameworks: Insights from the Z-Scan Technique

Rashi M. Patil[1], Tanmay P. Jagtap[2], Suhas R Patil[3], Kavita Patil[4], Ganesh Nehare[5], Shobha Waghmode[2], U.D.Patil[6], D.M.Nerkar[7], Madhav Rajwade[7*]

[1]Department of Applied Physics, Defence Institute of Advanced Technology, DU, DRDOPune-411025, India

[2] Department of Chemistry MES Abasaheb Garware College, Pune-411004, India

[3]Department of Physics, Dr. Annasaheb G. D. Bendale Mahila Mahavidyalaya, Jalgaon 425001

[4]Department of Physics and Electronics, KCE Society's Moolji Jaitha College (Autonomous), Jalgaon 425001

[5]Department of Chemistry, Sheth J. N. Paliwala Commerce, Science and Arts College, Pali, Raigad.

[6]Department of Physics, Annasaheb Awate College, Manchar 410503

[7]Department of Physics, PTVA's Sathaye College, Dixit Road, Vile Parle (East), Mumbai 400057

Corresponding author: madhavr64@gmail.com

Article History:

Received:12-08-2025

Revised:10-09-2025

Accepted:25-10-2025

Abstract:

Metal-organic frameworks (MOFs) are a type of porous material that can be changed in shape and used for many different purposes. This makes them perfect for nonlinear optical (NLO) applications. This study examines the nonlinear optical characteristics of a newly synthesized metal-organic framework (MOF), Mn-NBDC, utilizing the Z-scan method. Both open- and closed-aperture Z-scan tests to get the nonlinear absorption coefficient (β) and the nonlinear refractive index (n_2). The open-aperture findings show substantial nonlinear absorption, which is caused by saturable absorption processes. Closed-aperture data indicate intensity-dependent nonlinear refraction, with a clear peak-valley signature in the transmittance curve, suggesting self-defocusing behavior. These findings highlight Mn-NBDC's potential in applications like optical limiting, laser safety, and photonic devices.

Keywords: Nonlinear Optics (NLO), Z-scan, MOF, Mn-NBDC, Optical Limiting

1. Introduction

Metal-organic framework (MOF) was synthesized from Metal nodes and organic spacers. Metal-organic frameworks (MOF) are a class of porous material composed of organic struts linked with inorganic metal nodes[1][2]. MOFs have been studied extensively, and due to the wide variety of organic spacers, they may be tailored to many applications such as gas storage

and separation, catalysis, and chemical sensing[3][4]. Metal-Organic Frameworks (MOFs) exhibit highly tunable structural features ideal for Z-scan characterization, offering valuable insights into their nonlinear optical properties[1][5]. The Manganese Acetate and 2-Amino Terephthalic acid MOF synthesized using a microwave-assisted method is particularly noteworthy. Its unique structure comprises robust Mn clusters connected via amino terephthalic acid linkers, forming a highly ordered 3D framework with exceptional thermal and chemical stability[6]. The uniform pore sizes and high surface area allow precise control of light-matter interactions[7]. These features enable the MOF to exhibit strong nonlinear optical responses, such as reverse saturation absorption or optical limiting, making it ideal for photonic and laser-based applications[8][9].

The Mn-NBDC (manganese-nitrobenzene-1,4-dicarboxylic acid) combination is ideal for nonlinear optical (NLO) applications due to the synergistic properties of its components. Manganese, as a transition metal, offers multiple oxidation states and coordination geometries, enabling a versatile framework with high stability[10]. Nitrobenzene-1,4-dicarboxylic acid (NBDC) acts as a ligand with strong π-conjugation and electron-withdrawing nitro groups, crucial for enhancing the material's polarizability and charge-transfer efficiency, the key factors in NLO activity. The rigid aromatic backbone of NBDC also ensures a stable framework with minimal structural distortions[11]. Together, Mn-NBDC forms a robust MOF with a high degree of symmetry, uniformity, and tailored electronic properties, making it highly suitable for NLO applications[12]. The Mn-NBDC material offers significant advantages and unique properties for nonlinear optical (NLO) applications. The nitro groups in NBDC enhance polarizability and facilitate efficient charge transfer, yielding a strong NLO response such as second-harmonic generation (SHG) or reverse saturation absorption[13]. Its robust coordination framework ensures excellent thermal and chemical stability, making it suitable for challenging environments[14]. High symmetry and porosity enable uniform light-matter interactions, boosting NLO efficiency and allowing molecular tuning[15]. Additionally, Mn's redox activity introduces multifunctionality, such as photocatalysis or energy transfer. This material is cost-effective and environmentally sustainable, utilizing transition metals instead of rare-earth elements commonly used in NLO systems[16].

The Z-scan method is a widely used technique to measure the nonlinear optical (NLO) properties of materials[17]. It involves moving a sample along the Z-axis through the focal plane of a tightly focused laser beam while monitoring the transmitted light intensity[18]. In an open-aperture Z-scan, all transmitted light is collected to evaluate nonlinear absorption, such as reverse saturation absorption or multi-photon absorption[19]. In a closed-aperture Z-scan, an aperture in the detector path measures changes in beam divergence to assess nonlinear refraction, like self-focusing or self-defocusing[20]. By analysing intensity variations, the method provides quantitative information about the material's NLO coefficients[21]. The Z-scan method is particularly suitable for characterizing Metal-Organic Frameworks (MOFs) due to its ability to probe their unique nonlinear optical (NLO) properties with high precision[22]. MOFs often exhibit tunable electronic structures, high porosity, and strong charge-transfer interactions, which contribute to significant NLO effects such as nonlinear absorption and

refraction. The Z-scan technique effectively captures these effects by analysing light-matter interactions in a focused laser beam. Additionally, the method requires minimal sample preparation, making it ideal for MOFs with complex architectures. Its sensitivity to subtle optical changes ensures accurate characterization of MOFs' NLO coefficients, aiding in their optimization for photonic applications[20].

The nonlinear optical (NLO) properties of Mn-NBDC MOF are being investigated, focusing on nonlinear absorption (NLA) and nonlinear refraction (NLR). Saturable absorption (SA) is expected, where absorption decreases at higher intensities due to ground-state depletion. Nonlinear refraction is analysed through the closed-aperture Z-scan to determine whether the material exhibits self-focusing (positive NLR) or self-defocusing (negative NLR)[23]. Additionally, the third-order nonlinear susceptibility (χ^3) is evaluated to quantify both the real (refractive) and imaginary (absorptive) components of the material's nonlinear response[24].Considering previous studies on metal-organic frameworks (MOFs) and their NLO behavior, Mn-NBDC MOF is expected to exhibit significant third-order NLO properties due to metal-ligand charge transfer and quantum confinement effects. Similar MOF-based materials have demonstrated reverse saturable absorption (RSA) arising from excited-state absorption (ESA) or two-photon absorption (TPA), making them promising candidates for optical limiting applications[25]. Depending on local field effects and ligand-metal interactions, the material may exhibit either self-focusing or self-defocusing behavior, as observed in other transition metal-based MOFs[26]. The anticipated high χ^3 value reinforces the potential of Mn-NBDC MOF for photonic applications such as optical switching and limiting. These expected outcomes align with prior research on MOFs with transition metal centers, which have demonstrated strong NLO responses due to their delocalized electronic structures and high polarizability[27].

Various methods were used to examine the synthesised MOFs: powder X-ray diffraction (PXRD), scanning electron microscopy, Fourier Transform Infrared Spectroscopy (FTIR), UV-Visible spectrophotometer, photoluminescence spectroscopy, and continuous-wave Z-scan technique (Laser running at 532 nm CW). These approaches gave a thorough understanding of the mofs' structural, optical, and nonlinear optical properties. The Z-scan method is a widely used experimental method to measure intensity-dependent nonlinear susceptibilities of materials. It measures the intensity as a function of the sample position by letting the sample migrate over the axis of a focused Gaussian beam. The Z-scan curve gives the real and imaginary components of the third-order nonlinear susceptibility.

Materials and Methods.

All chemicals were used without further purification. Manganese(II) acetate tetrahydrate [$Mn(CH_3COO)_2 \cdot 4H_2O$, 99.8% purity] and 2-amino-1,4-benzenedicarboxylic acid (NH_2-BDC, 99.8% purity) were purchased from SRL Pvt. Ltd. Deionized (DI) water and absolute ethanol (analytical grade) were used as solvents throughout the synthesis to ensure a clean reaction medium and to minimize contamination. The selection of NH_2-BDC as an organic linker was based on its bifunctional nature, which promotes strong coordination with the metal centers,

while manganese was chosen for its known potential to contribute to magnetic and electronic properties in MOFs.

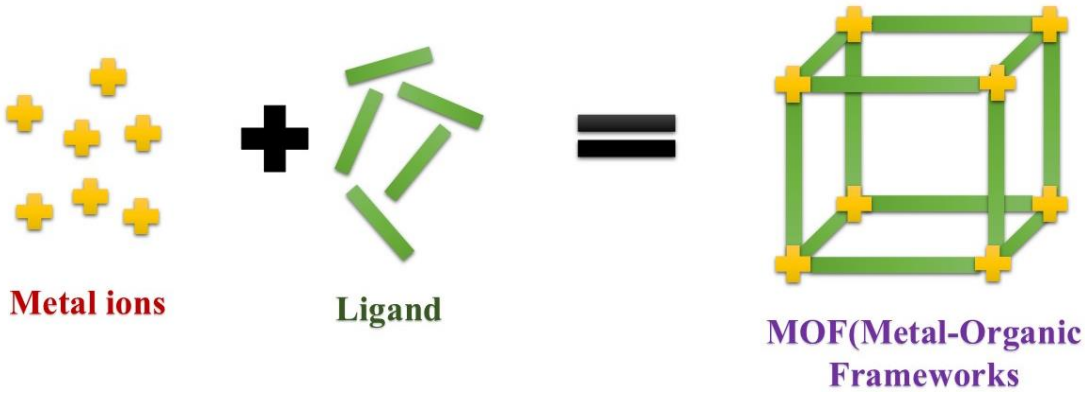

Figure 1: General reaction mechanism of MOFs synthesis

Synthesis Method

The Mn–NBDC metal–organic framework was synthesized using a microwave-assisted solvothermal technique, chosen for its rapid reaction time and improved crystallinity of the final product. As seen in Figure 1, a typical synthesis, 0.5 mmol of manganese(II) acetate tetrahydrate (0.123 g) and 0.5 mmol of 2-amino-1,4-benzenedicarboxylic acid (0.091 g) were dissolved in 20 mL of deionized water under magnetic stirring for 15 minutes to ensure complete dissolution. The resulting clear solution was transferred to a microwave-compatible reaction vessel.

The mixture was then subjected to microwave irradiation at 300 W for 10 minutes using a laboratory-grade microwave reactor. This rapid heating method ensures uniform temperature distribution and enhances nucleation and growth kinetics of the MOF crystals. After irradiation, the vessel was allowed to cool naturally to ambient temperature. The resulting suspension was filtered under vacuum to separate the solid product. The obtained precipitate was washed multiple times with ethanol and deionized water to remove unreacted precursors, residual solvents, and by-products. The purified material was then dried in a vacuum oven at 60 °C for 12 hours, ensuring complete removal of residual moisture and solvent molecules. The dried product appeared as a pale-yellow crystalline powder and was stored in a desiccator for further characterization. For the Z-scan measurements, 1 mg of the final MOF product was dissolved in 5 mL of DMF, and this resulting concentration was used for all experiments.

Characterization Methods

Different approaches of characterization were used to examine the produced MOFs. Bruker AXS D8 system using CuKα radiation (λ = 1.5404 Å) was used for powder X-ray diffraction (PXRD) studies. Over a 2θ range of 0–90°, the scans were carried out at 0.1°/min. Scanning electron microscopy (SEM-ZEISS) with an accelerating voltage of 2.00kV investigated the size and form of the MOFs. Surface functional groups were investigated using Fourier Transform Infrared Spectroscopy (FTIR, Perkin Elmer System 2000), which records spectra in the 400–4000 cm^{-1} range at room temperature. Using a UV-Visible spectrophotometer (Perkin

Elmer Lambda 25) throughout a wavelength range of 200–800 nm, the optical absorption properties were investigated; fluorescence qualities were found using photoluminescence spectroscopy (Ocean Optics tabletop setup). Furthermore, examined were the third-order nonlinear optical characteristics of the MOFs utilizing a continuous-wave Z-scan approach running a laser at 532 nm. These techniques together gave thorough understanding of the structural, optical, and nonlinear optical properties of the MOFs.

Experimental Setup to study the Nonlinearity

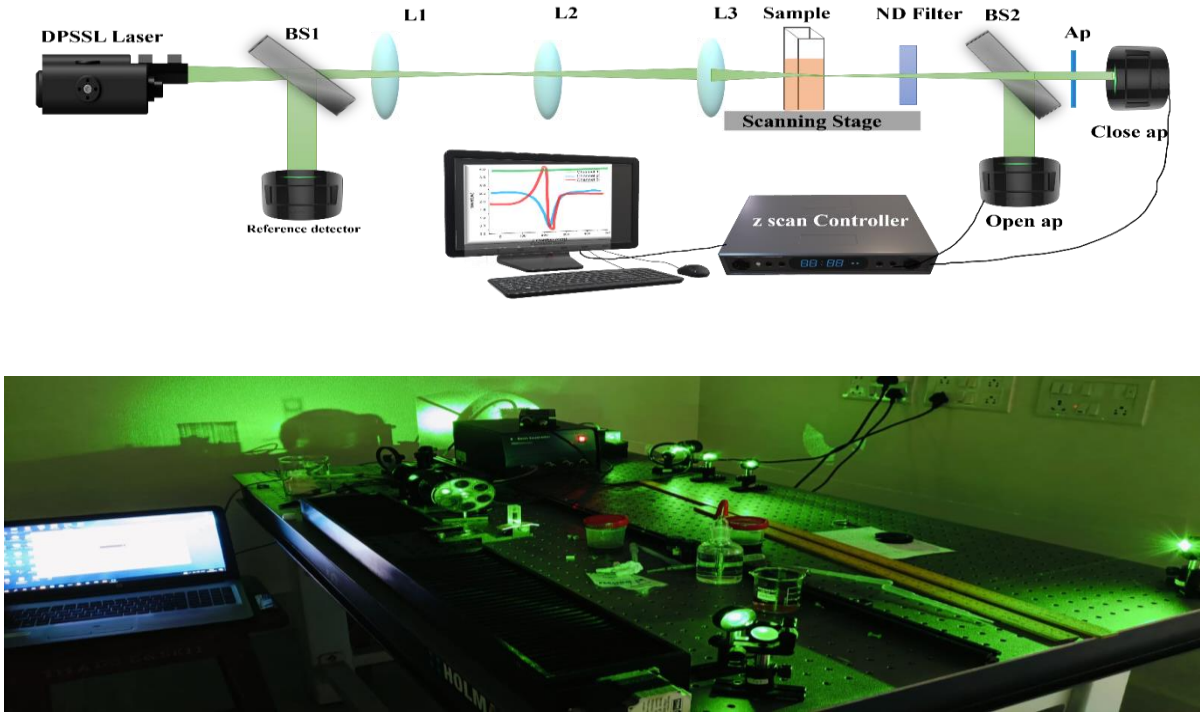

Figure 2: Layout and actual image of Z-scan experiment setup

From Figure 2, an extensively used experimental method to quantify intensity-dependent nonlinear susceptibilities of materials is the Z-scan method. This method measures the intensity as a function of the sample position by letting the sample migrate over the axis of a focused Gaussian beam. Predicted on a local response, analysis of the intensity against sample position, that is, the Z-scan curve, gives the real and imaginary components of the third-order nonlinear susceptibility. The working Z-scan configuration is briefly discussed. The sample was illuminated using a 532 nm ~100 mW DPSS laser. Initially, the laser energy was split 50:50 using a beam splitter. One arm pointed toward the reference detector (D1), while in the other working arm the beam was extended 1 cm with lenses (L1 and L2). M1 and M2 folded the beam even more, then directed it at L3 with a 100 mm focal length. The beam was also directed using ND filter and a beam splitter (BS2) to the detectors D2 and D3. Considered as the open aperture (OA) Z-scan, the detector D2 gauges the intensity as received without any aperture. One 25mm aperture was positioned in front of detector D3, which logs closed aperture Z-scan data. The L3 and the detectors D2 and D3 lie around 85 cm apart. Placed in a cuvette, the sample solution was scanned across the beam focus under a motorized linear translational stage with a 1mm step size and up to a 40 cm range. Careful optical alignment was done and control

data was acquired using DI water (data not shown) prior to the real tests. This guarantees not only the precision of the optical alignment but also the absence of stray light landing on the detector that causes spectra in the dark room environment to be noisy.

Results and Discussion

Optical Characterization

Mn–NBDC shows a strong UV–Vis absorption peak at 366 nm. The optical band gap was evaluated using the Tauc relation. A clear linear region in the $(\alpha h\nu)^2$ plot (direct-allowed transition) shows a clear linear region, giving Eg≈3.09 eV. This absorption arises from ligand π–π, n–π and metal–ligand charge-transfer transitions, with additional π–π* bands below 300 nm and high transparency beyond 400 nm. Its PL spectrum spans 350–750 nm, peaking at 500–600 nm, reflecting efficient π–π* emission and charge-transfer interactions. As shown in Figure 3, the moderate PL intensity balances radiative decay and excited-state absorption, favoring two-photon absorption and optical limiting without excessive fluorescence loss. Strong UV absorption coupled with visible-region transparency and a likely non-centrosymmetric structure suggest Mn–NBDC is well suited for third-order NLO effects (e.g., Kerr modulation, THG) and potentially second-order processes (e.g., SHG). Time-resolved PL is recommended to quantify excited-state lifetimes and optimize NLO performance.

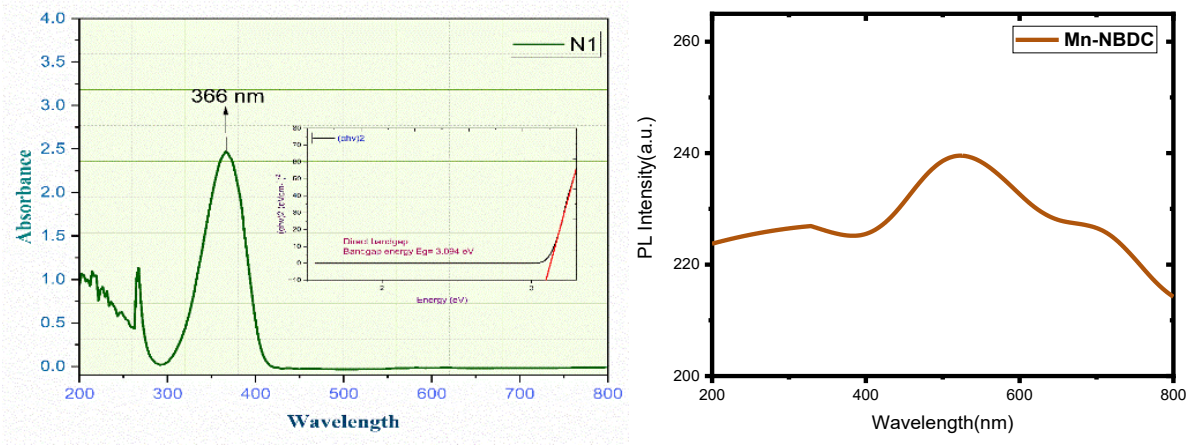

Figure 3: Absorption and emission spectra of MOFs

Structural Characterization:

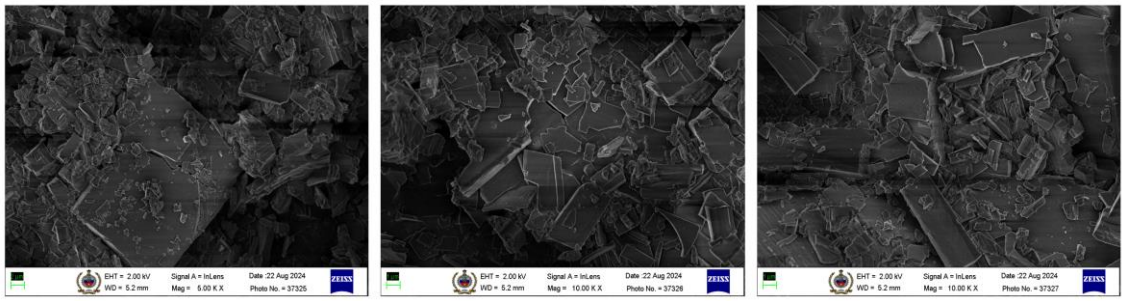

Figure 4: SEM images show MOFs morphology

The scanning electron microscopy (SEM) images in Figure 4, the synthesized Mn–NBDC MOF, captured at magnifications of 5,000× and 10,000×, reveal a well-defined crystalline morphology. The micrographs display the formation of densely packed plate-like and rod-like structures, indicative of a highly crystalline nature. The layered architecture and angular edges suggest uniform crystal growth, likely governed by the coordination between manganese centers and the organic linker (NH_2–BDC). The particles appear to be interconnected and closely stacked, which may contribute to the material's high surface area and porosity. No significant agglomeration or amorphous regions are observed, confirming the effectiveness of the microwave-assisted synthesis method in producing a homogeneous and structurally ordered MOF. These morphological features are consistent with materials designed for nonlinear optical and adsorption-based applications.

FTIR Analysis:

The N1 MOF's FT-IR spectrum has distinctive peaks that offer information about its structural makeup. Absorbing bands in the 3500–3300 cm^{-1} range indicate the existence of nitrogen-containing organic linkers via corresponding asymmetric and symmetric stretching vibrations of amine (-NH_2). C=O stretching is linked to a clear peak at 1700–1600 cm^{-1} that suggests the presence of carbonyl functional groups, most likely from carboxylate ligands. Furthermore, a peak close to 1600 cm^{-1} corresponds to C=C stretching as shown in Figure 5, thereby verifying the presence of aromatic or conjugated bonds, which are very typical in MOF structures. Attributed to C–N stretching, the peak at around 1400 cm^{-1} supports the existence of nitrogen-rich organic ligands even more. Especially the lower wavenumber area (below 1000 cm^{-1}) shows peaks matching metal-nitrogen (M–N) and metal-oxygen (M–O) bonding, therefore supporting the effective coordination between metal centers and organic ligands. Indicating a well-structured framework with strong metal-ligand interactions, these spectrum characteristics together corroborate the development of the N1 MOF.

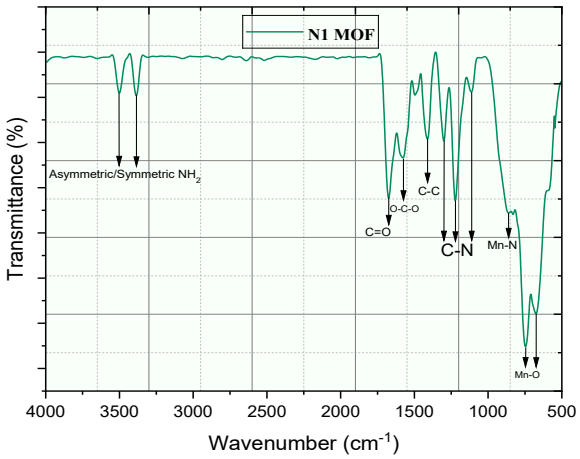

Figure 5: Available surface functional group over MOFs

Experimental data and analysis

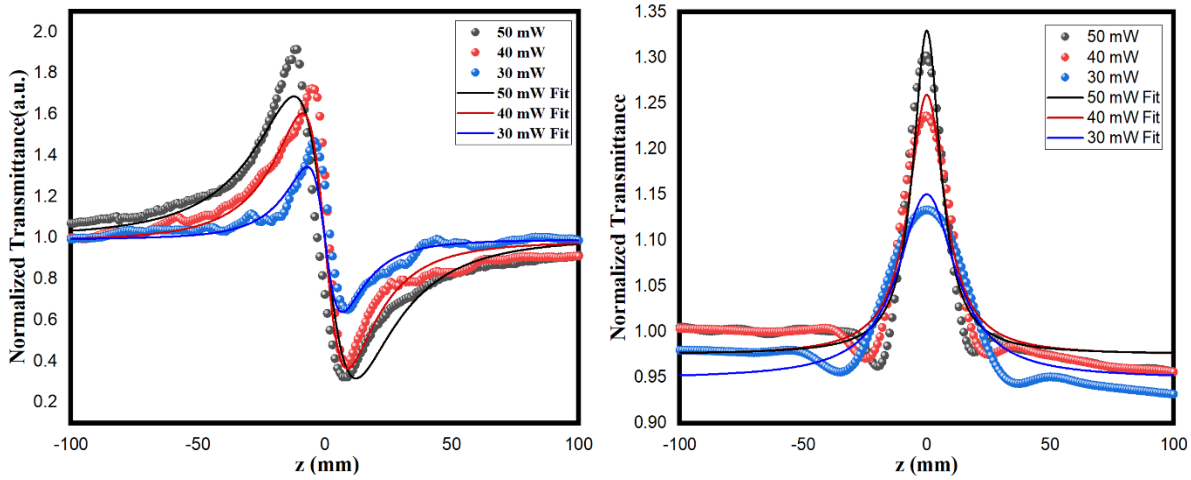

Figure 6: Close aperture and Close aperture data plots with variations of intensity of MOFs

Z-scan measurements were performed using a continuous-wave (CW) laser to examine the sample's steady-state nonlinear absorption/refraction under low-intensity excitation. In Figure 6, the order to prevent artifacts from extremely high peak intensities, such as multiphoton absorption, excited-state absorption, or sample damage, pulsed sources (ns–fs) were avoided. Z-scan traces were recorded at various input intensities, thin samples, and low incident powers were used to minimize and evaluate potential thermal contributions, and it was discovered that the nonlinear coefficients scaled as anticipated for an instantaneous (electronic) response. The measured nonlinear optical parameters are primarily of non-thermal origin, as evidenced by the absence of any time lag upon beam modulation.

Closed-Aperture Z-scan

The MOFs were subjected to a Z-scan experiment to determine the nonlinear responses of the samples and were recorded. For each sample, the experiment was repeated 5 times to check the repeatability. All MOFs recorded with different synthesis methods showed different nonlinear responses both in CA and OA scans. The closed-aperture Z-scan displays a peak-valley profile, characteristic of negative nonlinear refraction (self-defocusing). The peak-valley contrast is strongest at 50 mW and decreases with lower intensities, showing that the nonlinear refractive index also depends on the incident intensity. This suggests a third-order nonlinear refractive response. Figure 6 shows representative graphs with the appropriate fits for both closed and open aperture data. Figure 6(left) shows closed aperture data. MOFs have shown superior nonlinear optical response, which is evident from $\Delta T_{p\text{-}v}$ values obtained from the graph. The values of the nonlinear phase shift ($\Delta\Phi$) were obtained from the curve fits and were substituted in the equation to determine the n_2 values of MOFs. The data can be fitted with the transmission function for closed-aperture Z-scan:

$$T_{\text{close}}(z) = 1 + \frac{4\Delta\Phi\left(\frac{z}{z_0}\right)}{\left(1 + \left(\frac{z}{z_0}\right)^2\right)\left(9 + \left(\frac{z}{z_0}\right)^2\right)}$$

The n_2 values thus estimated are 3.865×10^{-10} m^2/W, respectively. This value can be substituted in the following equation to obtain a nonlinear refractive index.

$$n_2 = \frac{\Delta \Phi \lambda}{2\pi I_0 L_{eff}}$$

The negative n_2 value of the samples represents the self-defocusing effect at the sample plane.

Open-Aperture Z-scan

The OA Z-scan data of MOFs are shown in Figure 6 (right), which shows the properties of NLA. All the MOFs have shown the behavior of saturable absorption at the intensity of I_0 = 35mW. To further investigate the intensity-dependent nonlinear response, measurements were conducted at varying intensities of 50 mW, 40 mW, and 30 mW. A clear change in nonlinear behavior was observed with Variations in intensity, and it was noted that the nonlinear response decreased with decreasing intensity. The open-aperture Z-scan shows saturable absorption (SA), with the transmittance peak around the focus becoming sharp at higher laser intensities. This indicates that the nonlinear absorption increases with increasing intensity. As the intensity decreases from 50 mW to 30 mW, the nonlinearity reduces, confirming an intensity-dependent SA behavior. All data was fitted with the open aperture the transmission of the beam through the sample can be mathematically represented as

$$T_{open}(z) = 1 - \frac{q_0}{\sqrt{8\left(1 + \left(\frac{z}{z_0}\right)^2\right)}}$$

By fitting this function to the experimental data. q_0 can be evaluated. This is related to β as:

$$\beta = \frac{q_0}{I_0 L_{eff}}$$

We have further calculated the NLA coefficient (β) from the ΔT values of the open aperture data. The value of the nonlinear absorption coefficient (β) is 1.341×10^{-3} to 0.882×10^{-3} mW. As the real and imaginary components of the linear susceptibility $\chi^{(1)}$ are associated with refraction and absorption, similarly, the real and imaginary parts of $\chi^{(3)}$ describe NLR and NLA. We have calculated the real and imaginary values of $\chi^{(3)}$, which are tabulated in Table 1 along with other relevant values.

These calculated values of n_2 and β can be employed to find the third-order nonlinear susceptibility ($\chi^{(3)}$). The real part of $\chi^{(3)}$ can be estimated using the following equation:

$$Re\chi^{(3)} = \frac{n_2 n_0^2 \varepsilon_0 c^2}{\pi}\left(\frac{m^2}{W}\right)$$

where ε_0 is the electric permittivity. Moreover, the imaginary counterpart can be found out by:

$$Im\chi^{(3)} = \frac{\beta n_0^2 \varepsilon_0 c^2 \lambda}{4\pi^2}(m/W)$$

After measuring both components, the real part of the third-order susceptibility, $\chi^{(3)\prime}$, is derived from the nonlinear refractive index (n_2) via the change in transmittance in the closed-aperture Z-scan. The imaginary part, $\chi^{(3)\prime\prime}$, is obtained from the nonlinear absorption coefficient (β) measured in the open-aperture Z-scan. To calculate the overall magnitude of the third-order susceptibility, $|\chi^{(3)}|$, we take the root-mean-square of these two components:

$$|\chi^{(3)}| = \sqrt{(\chi^{(3)\prime})^2 + (\chi^{(3)\prime\prime})^2}$$

expressed in electrostatic units (esu). This RMS value represents the material's total third-order nonlinear response.

The results can be tabulated as follows:

Table 1: Nonlinear optical parameters of the synthesized Mn-NBDC MOFs

Parameters	**Values**
Laser Wavelength	532 nm
Lens focal length	250 mm
Rayleigh Range (z_0)	1.48 m
Beam radius at focus (ω_0)	2.5 mm
Radius of aperture	1.25 mm
Sample thickness (L)	1 cm

Intensity	50mw	40mw	30mw
Nonlinear Phase Shift ($\Delta\Phi$)	3.15536	3.0520	2.94183
Nonlinear absorption co-efficient, β (m/W)	1.341×10^{-3}	1.283×10^{-3}	0.882×10^{-3}
Nonlinear refractive index, n_2 (m^2/W)	3.502×10^{-10}	3.285×10^{-10}	2.996×10^{-10}
Real part of third-order susceptibility, $Re(\chi^{(3)})$ (esu)	7.5803×10^{-13}	7.110×10^{-13}	6.4850×10^{-13}
Imaginary part of third-order susceptibility, $Im(\chi^{(3)})$ (esu)	3.0737×10^{-14}	2.9407×10^{-14}	2.02164×10^{-14}
Third-order nonlinear susceptibility, $\chi^{(3)}$ (esu)	7.5865×10^{-13}	7.1160×10^{-13}	6.4881×10^{-13}

From these measurements, key third-order nonlinear parameters were extracted. The nonlinear absorption coefficient (β) ranged from 1.341×10^{-3} m/W at 50 mW to 0.882×10^{-3} m/W at 30 mW. Similarly, the nonlinear refractive index (n_2) decreased from 3.502×10^{-10} m²/W to 2.996×10^{-10} m²/W. The third-order nonlinear susceptibility components also followed this trend: the real part $\mathrm{Re}(\chi^{(3)})$ and imaginary part $\mathrm{Im}(\chi^{(3)})$ reduced as intensity dropped. The overall third-order susceptibility $|\chi^{(3)}|$ decreased from 7.5865×10^{-13} esu at 50 mW to 6.4881×10^{-13} esu at 30 mW, clearly illustrating that the nonlinear response of Mn-NBDC MOFs is intensity-dependent and dominated by third-order effects.

Conclusion

We have successfully synthesized a crystalline Mn–NBDC metal–organic framework via a rapid microwave-assisted solvothermal method and performed comprehensive characterization, including SEM, UV–Vis, and photoluminescence analyses to confirm its morphology, optical band gap, and broad emission profile. Z-scan measurements in DMSO solution revealed pronounced third-order nonlinear optical behavior, quantified by significant values of the nonlinear refractive index (n_2) and absorption coefficient (β), yielding an overall third-order susceptibility $|\chi^{(3)}|$ in the 10^{-7} esu range. Because our measurements were conducted on nanoplate suspensions (100 nm–1 μm), only third-order effects were observed. If larger, bulk crystals can be grown, direct Kerr-effect experiments could be performed to probe second-order nonlinearity (e.g., SHG). Future work will focus on optimizing crystal size and exploring solid-state measurements to unlock both second- and third-order nonlinearities for advanced photonic applications.

Acknowledgments

The authors gratefully acknowledge MES Abasaheb Garware College for providing the laboratory space and resources for the synthesis of the Mn–NBDC framework. We thank the Defence Institute of Advanced Technology (DIAT) for access to their z-scan setup and comprehensive characterization facilities. The authors recognize the support of DST-FIST at Garware College, as well as MJPRF-Nagpur.

References

[1] W. Shi, X. Xu, L. Zhang, W. Liu, and X. Cao, “Metal-organic framework-derived structures for next-generation rechargeable batteries,” *Functional Materials Letters*, vol. 11, no. 6, Dec. 2018, doi: 10.1142/S1793604718300062.

[2] P. Jagtap Tanmay, G. Sharda, and A. Waghmode Shobha, “The Atmospheric water harvesting by using Neodymium Metal Organic Framework (MOF-417),” *Research Journal of Chemistry and Environment*, vol. 28, no. 9, pp. 43–46, Sep. 2024, doi: 10.25303/289rjce043046.

[3] Z. Liang, R. Zhao, T. Qiu, R. Zou, and Q. Xu, “Metal-organic framework-derived materials for electrochemical energy applications,” Jul. 01, 2019, *Elsevier B.V.* doi: 10.1016/j.enchem.2019.100001.

[4] T. P. Jagtap, R. M. Patil, P. Deokar, and S. A. Waghmode, “Metal-Organic Frameworks as Electrode Materials for Lithium-Ion Battery,” *Science of Advanced Materials*, vol. 16, no. 9, pp. 923–940, Jun. 2024, doi: 10.1166/sam.. 2024.4715.

[5] R. M. Patil, A. Raj R, S. Mondal, T. Bhave, and A. V. R. Murthy, “An Analytical Disquisition on the Nonlinear Optical Responses of Carbon Quantum Dots Engineered by Diverse Synthesis Methodologies,” *Nano Trends*, p. 100081, Jan. 2025, doi: 10.1016/J.NWNANO.2025.100081.

[6] Y. Sakamaki *et al.*, “Preparation and Applications of Metal-Organic Frameworks (MOFs): A Laboratory Activity and Demonstration for High School and/or Undergraduate Students,” *Journal of Chemical Education*, vol. 97, no. 4, pp. 1109–1116, Apr. 2020, doi: 10.1021/acs.jchemed.9b01166.

[7] P. Falcaro *et al.*, “A new method to position and functionalize metal-organic framework crystals,” *Nature Communications*, vol. 2, no. 1, 2011, doi: 10.1038/ncomms1234.

[8] G. Zhang, H. Zheng, M. Shen, L. Wang, and X. Wang, “Green synthesis and characterization of Au@Pt core–shell bimetallic nanoparticles using gallic acid,” *Journal of Physics and Chemistry of Solids*, vol. 81, pp. 79–87, Jun. 2015, doi: 10.1016/J.JPCS.2014.12.012.

[9] C. Li, G. Qian, and Y. Cui, “Metal--organic frameworks for nonlinear optics and lasing,” *Information \& Functional Materials*, vol. 1, no. 2, pp. 125–159, 2024.

[10] S. Natarajan and S. Mandal, “Open-Framework Structures of transition-metal compounds,” *Angewandte Chemie International Edition*, vol. 47, no. 26, pp. 4798–4828, 2008.

[11] L. Yang *et al.*, “Metal--organic frameworks constructed from tib and carboxylate acid ligands: selective sensing of nitro explosives and magnetic properties,” *Dalton Transactions*, vol. 46, no. 23, pp. 7567–7576, 2017.

[12] Ummah, Masfi Sya’fiatul. "Pengalaman Perawat Dalam Melaksanakan Asuhan Keperawatan Dengan Metode Tim Di Ruang Rawat Inap Rsud Dr. Slamet Garut." Jurnal Sustainability 11.1 (2019): 1-14.

[13] H. Ghasempour *et al.*, “Metal–organic frameworks based on multicarboxylate linkers,” 2021. doi: 10.1016/j.ccr.2020.213542.

[14] Y. Hu *et al.*, “Recent advance of graphene/semiconductor composite nanocatalysts: Synthesis, mechanism, applications and perspectives,” *Chemical Engineering Journal*, vol. 414, p. 128795, Jun. 2021, doi: 10.1016/J.CEJ.2021.128795.

[15] W. Xiang, Y. Zhang, H. Lin, and C. J. Liu, “Nanoparticle/metal-organic framework composites for catalytic applications: Current status and perspective,” Dec. 01, 2017, *MDPI AG*. doi: 10.3390/molecules22122103.

[16] S. Shi *et al.*, "Full microwave synthesis of advanced Li-rich manganese based cathode material for lithium ion batteries," *Journal of Power Sources*, vol. 337, pp. 82–91, Jan. 2017, doi: 10.1016/j.jpowsour.2016.10.107.

[17] V. Singh *et al.*, "Measurements of third-order optical nonlinearity using Z-Scan technique: a review," in *AIP Conference Proceedings*, 2019, p. 140035.

[18] X. Du, C. Florian, and C. B. Arnold, "Single-lens dynamic z-scanning for simultaneous in situ position detection and laser processing focus control," *Light: Science \& Applications*, vol. 12, no. 1, p. 274, 2023.

[19] Y. Liang *et al.*, "Investigation on the optical nonlinearity of the layered magnesium-mediated metal organic framework (Mg-MOF-74)," *Optics Express*, vol. 29, no. 15, p. 23786, 2021, doi: 10.1364/oe.432234.

[20] V. Siva, A. Shameem, A. Murugan, S. Athimoolam, G. Vinitha, and S. A. Bahadur, "Structural, thermal and electro-optical properties of guanidine based Metal-Organic Framework (MOF)," *Chinese Journal of Physics*, vol. 68, pp. 764–777, 2020, doi: 10.1016/j.cjph.2020.09.036.

[21] R. Abazari *et al.*, "Third-Order Nonlinear Optical Behavior of an Amide-Tricarboxylate Zinc(II) Metal-Organic Framework with Two-Fold 3D+3D Interpenetration," *Inorganic Chemistry*, vol. 60, no. 13, pp. 9700–9708, 2021, doi: 10.1021/acs.inorgchem.1c00997.

[22] E. W. Van Stryland and M. Sheik-Bahae, "Z-scan," in *Characterization techniques and tabulations for organic nonlinear optical materials*, Routledge, 2018, pp. 671–708.

[23] E. W. Van Stryland and D. J. Hagan, "Measuring nonlinear refraction and its dispersion," in *Self-focusing: Past and Present: Fundamentals and Prospects*, Springer, 2009, pp. 573–591.

[24] S. S. Shinde, M. C. Sreenath, S. Chitrambalam, I. H. Joe, and N. Sekar, "Spectroscopic, DFT and Z-scan approach to study linear and nonlinear optical properties of Disperse Red 277," *Optical Materials*, vol. 99, no. August, p. 109536, 2020, doi: 10.1016/j.optmat.2019.109536.

[25] L. Zeng, X.-Y. Wang, N. Li, J. Pang, and X.-H. Bu, "Low-power, non-coherent light-triggered two-photon absorption via extending the lifetime of the transition state," *Coordination Chemistry Reviews*, vol. 511, p. 215868, 2024.

[26] F. S. Richardson, "Theory of optical activity in the ligand-field transitions of chiral transition metal complexes," *Chemical Reviews*, vol. 79, no. 1, pp. 17–42, 1979.

[27] B. Ni, W. Sun, J. Kang, and Y. Zhang, "Understanding the linear and second-order nonlinear optical properties of UiO-66-derived metal--organic frameworks: A comprehensive DFT study," *The Journal of Physical Chemistry C*, vol. 124, no. 21, pp. 11595–11608, 2020.